PHYSICAL REVIEW D **86**, 095011 (2012)

Discovering new gauge bosons of electroweak symmetry breaking at LHC-8

Chun Du,[1] Hong-Jian He,[1,2] Yu-Ping Kuang,[1] Bin Zhang,[1] Neil D. Christensen,[3]
R. Sekhar Chivukula,[4] and Elizabeth H. Simmons[4]

[1]*Center for High Energy Physics, Tsinghua University, Beijing 100084, China*
[2]*Theory Division, CERN, CH-1211 Geneva 23, Switzerland*
[3]*Pittsburgh Particle Physics, Astrophysics and Cosmology Center, Department of Physics and Astronomy, University of Pittsburgh, Pittsburgh, Pennsylvania 15260, USA*
[4]*Department of Physics and Astronomy, Michigan State University, East Lansing, Michigan 48824, USA*

(Received 27 June 2012; published 8 November 2012)

We study the physics potential of the 8 TeV LHC (LHC-8) to discover, during its 2012 run, a large class of extended gauge models or extradimensional models whose low-energy behavior is well represented by an $SU(2)^2 \otimes U(1)$ gauge structure. We analyze this class of models and find that, with a combined integrated luminosity of 40–60 fb^{-1} at the LHC-8, the first new Kaluza-Klein mode of the W gauge boson can be discovered up to a mass of about 370–400 GeV when produced in association with a Z boson.

DOI: 10.1103/PhysRevD.86.095011 PACS numbers: 12.60.Cn, 11.10.Kk, 12.15.Ji, 13.85.Qk

I. INTRODUCTION

By the end of 2011, the LHC, running at a center-of-mass energy of 7 TeV, had accumulated an integrated luminosity of about 5 fb^{-1} from both the ATLAS and CMS experiments [1]. Since April 5, 2012, the LHC has been running at an 8 TeV collision energy, and has collected about 12 fb^{-1} of data in each detector as of August 20. The LHC, running in this "LHC-8" mode, is expected to produce up to about 20–30 fb^{-1} of data apiece in the ATLAS and CMS detectors by the end of this year, which will amount to 40–60 fb^{-1} in total. This will enable the LHC to make incisive tests of the predictions of many competing models of the origin of electroweak symmetry breaking (EWSB), ranging from the Standard Model (SM) with a single Higgs boson, to models with multiple Higgs bosons, and to so-called Higgsless models of the EWSB. The Higgsless models [2] contain new spin-1 gauge bosons, which play a key role in EWSB by delaying the unitarity violation of longitudinal weak boson scattering up to a higher ultraviolet (UV) scale [3] without invoking a fundamental Higgs scalar. Very recently, the effective UV completion of the minimal three-site Higgsless model [4] was presented and studied in Ref. [5], which showed that the latest LHC signals of a Higgs-like state with mass around 125–126 GeV [6] can be readily explained, in addition to the signals of new spin-1 gauge bosons studied in the present paper.

In this work, we explore the physics potential of the LHC-8 to discover a relatively light fermiophobic electroweak gauge boson W_1 with mass 250–400 GeV, as predicted by the minimal three-site moose model [4] and its UV completion [5]. Being fermiophobic or nearly so, the W_1 state is allowed to be fairly light. More specifically, the 5D models that incorporate ideally [7] delocalized fermions [8,9], in which the ordinary fermions propagate appropriately in the compactified extra dimension (or, in deconstructed language, derive their weak properties from more than one $SU(2)$ group in the extended electroweak sector [10,11]), yield phenomenologically acceptable values for all Z-pole observables [4]. In this case, the leading deviations from the SM appear in multi-gauge boson couplings, rather than the oblique parameters S and T. Reference [12] demonstrates that the LEP-II constraints on the strength of the coupling of the Z_0-W_0-W_0 vertex allow a W_1 mass as light as 250 GeV, where W_0 and Z_0 refer to the usual electroweak gauge bosons.

In the next section we introduce the model. Section III presents our analysis of the $pp \to W_1 Z_0 \to W_0 Z_0 Z_0 \to jj\ell^+\ell^-\ell^+\ell^-$ process at the LHC-8. Finally, we demonstrate that the LHC-8 should be able to sensitively probe W_1 bosons in the mass range of 250–400 GeV by the end of this year.

II. THE MODEL

We study the minimal deconstructed moose model at LHC-8 in a limit where its gauge sector is equivalent to the "three-site model" [4] or its UV-completed "minimal linear moose model" (MLMM) [5], whose gauge boson phenomenology was previously studied [13,14] for the 14 TeV LHC. Both the three-site model and the MLMM are based on the gauge group $SU(2)_0 \otimes SU(2)_1 \otimes U(1)_2$, as depicted by Fig. 1, and its gauge sector is the same as that of the breaking electroweak symmetry strongly (BESS) models [15,16] or the hidden local symmetry model [17–21]. The extended electroweak symmetry spontaneously breaks to electromagnetism when the distinct Higgs link fields Φ_1, connecting $SU(2)_0$ to $SU(2)_1$, and Φ_2, connecting $SU(2)_1$ to $U(1)_2$, acquire vacuum expectation values (VEVs), $f_{1,2}$. The weak scale $v \simeq 246$ GeV is related to those VEVs via $v^{-2} = f_1^{-2} + f_2^{-2}$ and, for illustration, we take $f_1 = f_2 = \sqrt{2}v$. Below the symmetry-breaking scale, the gauge boson spectrum includes an extra set of weak bosons (W_1, Z_1), in addition to the Standard

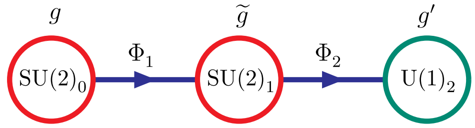

FIG. 1 (color online). Moose diagram of the MLMM with the gauge structure $SU(2)_0 \times SU(2)_1 \times U(1)_2$ as well as two independent link fields Φ_1 and Φ_2 for spontaneous symmetry breaking. The relevant parameter space of phenomenological interest is where the gauge couplings obey $g, g' \ll \tilde{g}$.

Model-like weak bosons (W_0, Z_0) and the photon. Furthermore, the scalar sector of the MLMM [5] contains two neutral physical Higgs bosons (h^0, H^0), as well as the six would-be Goldstones eaten by the corresponding gauge bosons (W_0, Z_0) and (W_1, Z_1).

In our previous work [13] on the phenomenology of such spin-1 new gauge bosons at a 14 TeV LHC, we studied the potential for detecting the W_1 via both the weak boson fusion $pp \to W_0 Z_0 jj \to W_1 jj \to W_0 Z_0 jj$ and the associated production process $pp \to W_1 Z_0 \to W_0 Z_0 Z_0$. Focusing on the mass range 400–1000 GeV, we found that associated production would require less integrated luminosity than the gauge boson fusion channel at the lower end of that mass range, as shown in Fig. 4 of Ref. [13]. Extrapolating that result to lower W_1 masses and a lower LHC collision energy, we have found in this work that for the LHC-8, the best process for detecting W_1 in the mass range 250–400 GeV is also the associated production, $pp \to W_1 Z_0 \to W_0 Z_0 Z_0 \to jj\ell^+\ell^-\ell^+\ell^-$, where we select the W_0 decays into dijets and the Z_0 decays into electron or muon pairs.

One distinctive feature of the MLMM is that the unitarity of high-energy longitudinal weak boson scattering is maintained jointly by the exchange of both the new spin-1 weak bosons and the spin-0 Higgs bosons [5]. This differs from either the SM (in which the unitarity of longitudinal weak boson scattering is ensured by the exchange of the Higgs boson alone) [22] or the conventional Higgsless models (in which the unitarity of longitudinal weak boson scattering is ensured by the exchange of spin-1 new gauge bosons alone) [3]. It has been shown [12] that the scattering amplitudes in such highly deconstructed models with only three sites can accurately reproduce many aspects of the low-energy behavior of 5D continuum theories.

The original Lagrangian of the three-site model is given in a nonlinear Higgsless form [4]:

$$\mathcal{L}_{\rm HL} = \frac{1}{4}\,{\rm Tr}[f_1^2(D_\mu\Sigma_1)^\dagger(D^\mu\Sigma_1) + f_2^2(D_\mu\Sigma_2)^\dagger(D^\mu\Sigma_2)], \tag{1}$$

where the nonlinear sigma fields $\Sigma_j = \exp[i\pi_j^a\tau^a/f_j]$ and τ^a denotes the Pauli matrices. The gauge covariant derivatives take the following forms:

$$D^\mu\Sigma_1 = \partial^\mu\Sigma_1 + igW_L^{a\mu}\frac{\tau^a}{2}\Sigma_1 - i\tilde{g}\Sigma_1 W_H^{a\mu}\frac{\tau^a}{2}, \tag{2a}$$

$$D^\mu\Sigma_2 = \partial^\mu\Sigma_2 + i\tilde{g}W_H^{a\mu}\frac{\tau^a}{2}\Sigma_2 - ig'\Sigma_2 W_R^{3\mu}\frac{\tau^3}{2}, \tag{2b}$$

where W_L, W_H, and W_R denote the gauge bosons of $SU(2)_0$, $SU(2)_1$, and $U(1)_2$, respectively.

Extending this construction, we will include the radial Higgs excitations in the sigma fields. We introduce the two radial Higgs excitations h_j as follows:

$$\Phi_j = (f_j + h_j)\Sigma_j, \qquad \Sigma_j = \exp[i\pi_j^a\tau^a/f_j], \tag{3}$$

where the Higgs fields Φ_j are 2×2 matrices, and the Higgs bosons $h_{1,2}$ are gauge singlets. Thus, we can write down the Lagrangian of the MLMM by including the radial Higgs excitations for Eq. (1),

$$\mathcal{L} = \frac{1}{4}\,{\rm Tr}[(D_\mu\Phi_1)^\dagger(D^\mu\Phi_1) + (D_\mu\Phi_2)^\dagger(D^\mu\Phi_2)] - V(\Phi_1, \Phi_2), \tag{4}$$

where $V(\Phi_1, \Phi_2)$ denotes the scalar potential as given in Ref. [5], but is not needed for the current study. In unitary gauge, this Lagrangian is identical to the renormalizable MLMM studied in Ref. [5]. Since our current phenomenological study (next section) focuses on the detection of spin-1 new gauge bosons in the MLMM, the radial Higgs excitations included in the Lagrangian [Eq. (4)] do not affect our collider analysis. For the following LHC analyses, we will always take $f_1 = f_2 = \sqrt{2}v$.

The unitarity of the generic longitudinal scattering amplitude of $W_0^L W_0^L \to W_0^L W_0^L$, in the presence of any numbers of spin-1 new gauge bosons $V_k(= W_k, Z_k)$ and spin-0 Higgs bosons h_k, was recently studied in Ref. [5]. It has been shown that requiring the exact cancellation of the asymptotic E^2 terms[1] in the scattering amplitude imposes the following sum rule on the couplings and masses [5]:

$$G_{4W_0} - \frac{3M_{Z_0}^2}{4M_{W_0}^2}G_{W_0W_0Z_0}^2 = \sum_k \frac{3M_{Z_k}^2}{4M_{W_0}^2}G_{W_0W_0Z_k}^2 + \sum_k \frac{G_{W_0W_0h_k}^2}{4M_{W_0}^2}. \tag{5}$$

Here $G_{V_iV_jV_k}$ is the cubic coupling among the three vector bosons indicated, Z_k is the kth Kaluza-Klein mode of the Z boson, and G_{4W_0} is the quartic coupling of W_0 bosons. Equation (5) extends the corresponding Higgsless sum rule derived in Ref. [23]. For the current MLMM, the general sum rule of Eq. (5) becomes [5]

[1]Here E denotes the center-of-mass energy of the relevant scattering process.

$$G_{4W_0} - \frac{3M_{Z_0}^2}{4M_{W_0}^2} G_{W_0W_0Z_0}^2 = \frac{3M_{Z_1}^2}{4M_{W_0}^2} G_{W_0W_0Z_1}^2 + \frac{G_{W_0W_0h}^2 + G_{W_0W_0H}^2}{4M_{W_0}^2}, \quad (6)$$

where the symbols (h, H) denote the two mass-eigenstate Higgs bosons, and we have $G_{W_0W_0h_1}^2 + G_{W_0W_0h_2}^2 = G_{W_0W_0h}^2 + G_{W_0W_0H}^2$. Because there is only a single extra set of weak gauge bosons in this theory, the sum over Kaluza-Klein modes on the right-hand side of Eq. (5) reduces to a single term. Then, with the Lagrangian of the MLMM [Eq. (4)], we have explicitly verified the sum rule [Eq. (6)]. Hence, the unitarity of longitudinal weak boson scattering in the MLMM is ensured jointly [5] by exchanging both the new spin-1 weak bosons W_1, Z_1 and the spin-0 Higgs bosons h, H. We also note that the hWW and hZZ couplings are generally suppressed [5] relative to the SM values because of the VEV ratio $f_2/f_1 = O(1)$ and the h-H mixing. As shown in Ref. [5], the MLMM can predict an enhanced diphoton rate for a light Higgs boson h with mass 125–126 GeV produced via gluon fusions, while the Higgs signals via associate production $q\bar{q}' \to hV_0$ and vector boson fusion $qq' \to hq''q'''$ (with $h \to b\bar{b}$, $\tau\bar{\tau}$) are always lower than in the SM.

III. ANALYSIS OF $W_1^{\pm}$ DETECTION AT THE LHC-8

In this section, we study the partonic-level signals and backgrounds for detecting $W_1^{\pm}$ states at the LHC-8 in the associated production channel. The signal events proceed via the process $pp \to W_1Z_0 \to W_0Z_0Z_0 \to jj\ell^+\ell^-\ell^+\ell^-$, where the leptons can be either electrons or muons. We have systematically computed all the major SM backgrounds for the $jj4\ell$ final state, including the irreducible backgrounds $pp \to W_0Z_0Z_0 \to jj4\ell$ $(jj = qq')$ without the contribution of W_1, as well as the reducible backgrounds $pp \to ggZ_0Z_0 \to jj4\ell$, $pp \to Z_0Z_0Z_0 \to jj4\ell$, and the SM $pp \to jj4\ell$ other than the above reducible backgrounds.

We performed the parton level calculations at tree level using two different methods and two different gauges to check the consistency. In one calculation, we used the helicity amplitude approach [24] to generate the signal and backgrounds. We also calculated both the signal and the background using CalcHEP [25,26]. For the signal calculation in CalcHEP, we used FeynRules [27] to implement the minimal Higgsless model [28]. We found satisfactory agreement between these two approaches and between both the unitary and 't Hooft-Feynman gauge. We used a scale of $\sqrt{\hat{s}}$ for the strong coupling in the backgrounds and $\sqrt{\hat{s}}/2$ for the CTEQ6L [29] parton distribution functions. We included both the first- and second-generation quarks in the protons and jets, and both electrons and muons in the final-state leptons.

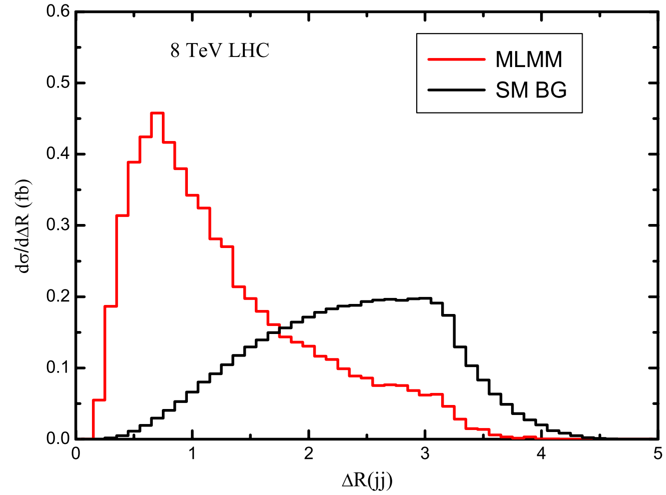

FIG. 2 (color online). Event distribution $\Delta R(jj)$ at LHC-8, for the MLMM with $M_{W1} = 300$ GeV (red curve with peak on the left-hand side), and for the SM backgrounds (black curve populated on the right-hand side) which peak around the large $\Delta R(jj)$.

In our calculations, we impose basic acceptance cuts,

$$p_{T\ell} > 10 \text{ GeV}, \qquad |\eta_\ell| < 2.5, \qquad p_{Tj} > 15 \text{ GeV}, \qquad |\eta_j| < 4.5, \quad (7)$$

and also a reconstruction cut for identifying W_0 bosons that decay to dijets,

$$M_{jj} = 80 \pm 15 \text{ GeV}. \quad (8)$$

The same cuts were imposed for our previous analysis for the 14 TeV LHC [13], where we found that a minimum-separation cut on the two jets was not necessary. We find that these cuts are also effective for $W_1^{\pm}$ searches at the LHC-8.

We further analyze the distributions of the dijet opening angle $\Delta R(jj)$ in the decays of $W_0 \to jj$ for both the signal and SM background events. This is depicted in Fig. 2. We find that the signal events are peaked in the small opening-angle region around $\Delta R(jj) \sim 0.6$, while the SM backgrounds tend to populate the range of larger opening angles, with a broad bump around $\Delta R(jj) = 1.5$–3.3. In order to sufficiently suppress the SM backgrounds, we find the following opening-angle cut[2] to be very effective [30]:

$$\Delta R(jj) < 1.6. \quad (9)$$

At the LHC-8, we note that the above cut reduces the signal events by only 10–15%, but removes about 72–80% of the SM backgrounds.

Next, we present the invariant-mass distribution $M(Z_0jj)$ in Fig. 3, where we compare the number of signal

[2] These are somewhat weaker than the cut of $\Delta R(jj) < 1.5$ imposed in Ref. [13].

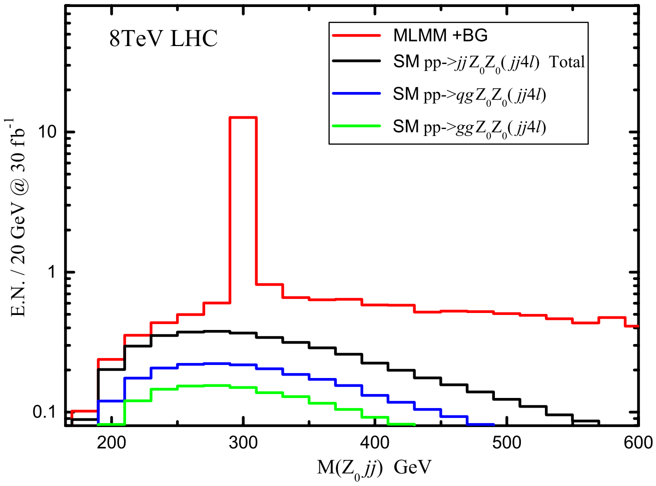

FIG. 3 (color online). Event number as a function of invariant mass $M(Z_0jj)$ after all relevant cuts. A $W_1^{\pm}$ boson of mass 300 GeV is used as a sample signal. The key of this plot identifies all curves in order from top to bottom.

events with all relevant SM backgrounds. We have used $M_{W1} = 300$ GeV as a sample value for a relatively light W_1 boson. Because the two Z_0 bosons are indistinguishable, each event is included twice, i.e., at the two $M(Z_0jj)$ values corresponding to the combination of each Z_0 boson with the dijets. The predicted signal events (plus SM backgrounds and the signal-derived combinatorial background) are shown for the MLMM (top red curve). We have systematically computed all the major SM backgrounds for the $jj4\ell$ final state, including the irreducible backgrounds $pp \to W_0Z_0Z_0 \to jj4\ell$ $(jj = qq')$ without the contribution of W_1, as well as the reducible backgrounds $pp \to qgZ_0Z_0 \to jj4\ell$ (blue curve, second from bottom), $pp \to ggZ_0Z_0 \to jj4\ell$ (green curve, bottom),

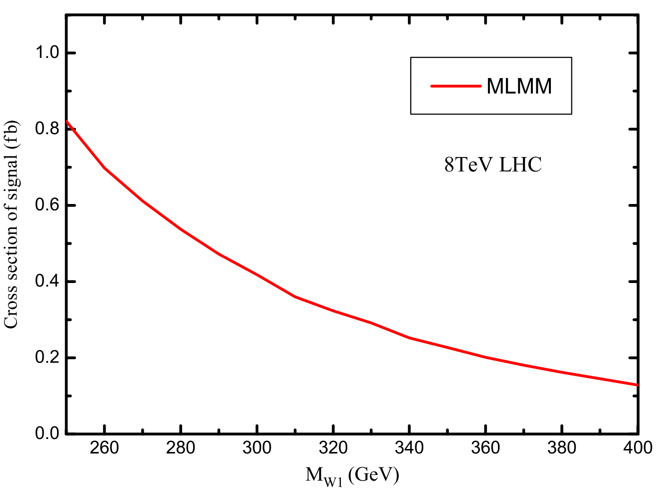

FIG. 4 (color online). Predicted signal cross section for $pp \to W_1Z_0 \to W_0Z_0Z_0 \to jj4\ell$ as a function of the W_1 mass in the MLMM after all cuts at the LHC-8.

TABLE I. Predicted signal cross sections of the MLMM and the SM backgrounds for $W_1^{\pm}$ production via $pp \to W_1Z_0 \to W_0Z_0Z_0 \to jj4\ell$ at the LHC-8, including all cuts described in the text.

M_{W_1} (GeV)	Signal cross section (fb)	Background cross sections (fb) $pp \to qgZ_0Z_0$	$pp \to ggZ_0Z_0$	Total
250	0.8205	0.0145	0.0101	0.0246
300	0.4180	0.0141	0.0096	0.0236
350	0.2271	0.0114	0.0078	0.0191
400	0.1282	0.0083	0.0058	0.0141

$pp \to Z_0Z_0Z_0 \to jj4\ell$ and other SM processes of the form $pp \to jj4\ell$. The summed total SM backgrounds are shown as the black curve (third from bottom) in Fig. 3. The irreducible background and the reducible backgrounds from $pp \to Z_0Z_0Z_0 \to jj4\ell$ and other SM $pp \to jj4\ell$ processes are so small that they are invisible in Fig. 3. We also note that the process $pp \to W_0^* \to W_0h^* \to W_0Z_0Z_0 \to jj4\ell$ is highly suppressed after all the cuts including Eq. (10) below, and is negligible in this analysis. From Fig. 3, we see that at LHC-8, the W_1 resonance peak is distinct and the SM backgrounds are effectively suppressed. For the light Higgs boson h^0 with mass around 125–126 GeV, the heavy gauge boson W_1 has a new decay channel $W_1 \to W_0h$, and its decay width relies on the Higgs mixing angle α. But it was found [5] that for our model with $f_1 = f_2$, the decay branching fraction of $W_1 \to W_0h$ is negligible relative to that of $W_1 \to W_0Z_0$ when the $h \to \gamma\gamma$ signals are consistent with the current LHC data [6].

In Fig. 4, we display the predicted total signal cross section for the process $pp \to W_0Z_0Z_0 \to jj4\ell$ after all cuts at the LHC-8 have been imposed; this is shown as a function of the W_1 mass for the range 250–400 GeV. Here, we define the signal region to include all events satisfying

$$M(Z_0jj) = M_{W_1} \pm 20 \text{ GeV}. \qquad (10)$$

The cross sections of signals and backgrounds are also listed in Table I for four sample values of W_1 masses, $M_{W_1} = 250, 300, 350, 400$ GeV.

IV. RESULTS AND CONCLUSIONS

Finally, we present the LHC-8 discovery reach for the relatively light W_1 mass range of 250–400 GeV. To calculate the statistical significance, we use the Poisson distribution, which governs the random generation of uncorrelated events. If the number of events expected in the background is ν, then the probability $P_P(n, \nu)$ that the number of events measured will fluctuate up to n is given by

$$P_P(n, \nu) = \frac{\nu^n e^{-\nu}}{n!}. \qquad (11)$$

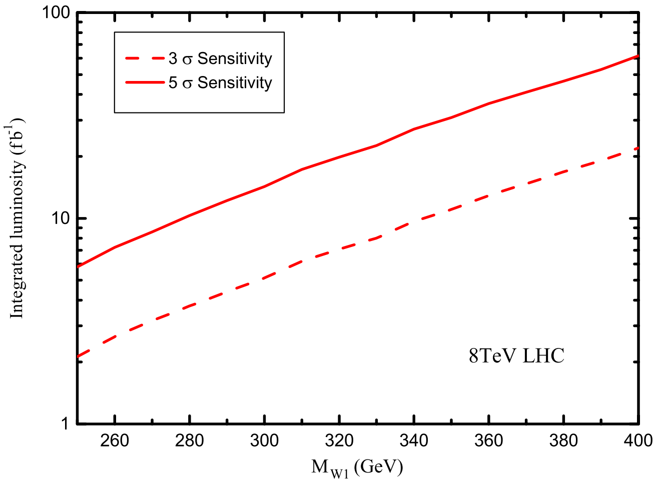

FIG. 5 (color online). Integrated luminosities required for the detection of new $W_1^{\pm}$ gauge bosons at the 3σ level in the MLMM (red dashed curve), and at the 5σ level (red solid curve) as a function of the W_1 mass, at the LHC-8.

TABLE II. The 5σ discovery reaches of the $W_1^{\pm}$ bosons at the LHC-8, with the integrated luminosities $\int \mathcal{L} = 10$, 15, 20, 25, 30, 35, 40, 50, 60 fb^{-1}, respectively.

$\int \mathcal{L}$ (fb^{-1})	M_{W_1} (GeV)
10	277
15	302
20	320
25	335
30	346
35	357
40	367
50	385
60	397

The probability that the background will fluctuate up to the background plus the signal or higher is then given by

$$P_P(n \geq \nu + s, \nu) = \sum_{n=\nu+s}^{\infty} \frac{\nu^n e^{-\nu}}{n!}. \qquad (12)$$

For this to correspond to a 3σ or 5σ significance, this probability must be the same as the probability for a Gaussian to fluctuate up 3 or 5 standard deviations, respectively: $P_G(3\sigma) = 0.00135$ or $P_G(5\sigma) = 2.87 \times 10^{-7}$ [31].

In Fig. 5, we display the required integrated luminosities for detecting the $W_1^{\pm}$ signal at the 3σ and 5σ levels as a function of the $W_1^{\pm}$ mass M_{W_1}. Table II summarizes the 5σ reach in M_{W_1} for some sample values of the integrated luminosity at the LHC-8. In this analysis, we have included statistical errors in determining the $W_1^{\pm}$ discovery potential. We anticipate that experimental analyses will include more complete detector level simulations, systematic errors and the details of detector geometry.

Figure 5 and Table II demonstrate that the LHC-8 should be able to probe the light-mass range for the $W_1^{\pm}$ gauge bosons quite effectively in the minimal linear moose model studied here. In fact, it has good potential for detecting $W_1^{\pm}$ with a mass below 400 GeV by the end of 2012. This is complementary to the discovery reach for heavier $W_1^{\pm}$ bosons (400 GeV–1 TeV) that our previous study [13] showed to be feasible for the LHC when running at 14 TeV collision energy.

In summary, the LHC-8 is continuing to test the origin of electroweak symmetry breaking. The minimally extended electroweak gauge structure of $SU(2)^2 \otimes U(1)$ generically predicts the extra spin-1 gauge bosons as the unambiguous new physics beyond the SM, which give distinct new signatures at the LHC. We have demonstrated that after the ATLAS and CMS detectors collect up to 30–60 fb^{-1} of data by the end of this year, the LHC-8 should have good potential to probe the dynamics of the extended gauge symmetry breaking $SU(2)^2 \otimes U(1) \to U(1)_{\rm em}$. We look forward to seeing the results.

ACKNOWLEDGMENTS

This research was supported by the NSF of China (Grants No. 10625522, No. 10635030, No. 11135003, No. 11075086, No. 11275101, and No. 11275102) and the National Basic Research Program of China (Grant No. 2010CB833000); by the U.S. NSF under Grants No. PHY-0854889 and No. PHY-0705682; and by the University of Pittsburgh Particle Physics, Astrophysics, and Cosmology Center. H. J. H. thanks the CERN Theory Division for hospitality.

[1] G. Aad *et al.* (ATLAS Collaboration), Phys. Lett. B **710**, 49 (2012); S. Chatrchyan *et al.* (CMS Collaboration), Phys. Lett. B **710**, 26 (2012).

[2] C. Csaki, C. Grojean, H. Murayama, L. Pilo, and J. Terning, Phys. Rev. D **69**, 055006 (2004); C. Csaki, C. Grojean, L. Pilo, and J. Terning, Phys. Rev. Lett. **92**, 101802 (2004).

[3] R. S. Chivukula, D. A. Dicus, and H. J. He, Phys. Lett. B **525**, 175 (2002); R. S. Chivukula and H. J. He, Phys. Lett. B **532**, 121 (2002); R. S. Chivukula, D. A. Dicus, H. J. He, and S. Nandi, Phys. Lett. B **562**, 109 (2003); H. J. He, Int. J. Mod. Phys. A **20**, 3362 (2005); R. S. Chivukula, H. J. He, M. Kurachi, E. H. Simmons, and M. Tanabashi, Phys. Rev. D **78**, 095003 (2008).

[4] R. S. Chivukula, B. Coleppa, S. Di Chiara, E. H. Simmons, H. J. He, M. Kurachi, and M. Tanabashi, Phys. Rev. D **74**, 075011 (2006).
[5] T. Abe, N. Chen, and H. J. He, arXiv:1207.4103 [J. High Energy Phys. (to be published)].
[6] G. Aad *et al.* (ATLAS Collaboration), Phys. Lett. B **716**, 1 (2012); S. Chatrchyan *et al.* (CMS Collaboration), Phys. Lett. B **716**, 30 (2012).
[7] R. S. Chivukula, E. H. Simmons, H. J. He, M. Kurachi, and M. Tanabashi, Phys. Rev. D **72**, 015008 (2005).
[8] G. Cacciapaglia, C. Csaki, C. Grojean, and J. Terning, Phys. Rev. D **71**, 035015 (2005).
[9] R. Foadi, S. Gopalakrishna, and C. Schmidt, Phys. Lett. B **606**, 157 (2005).
[10] R. S. Chivukula, E. H. Simmons, H. J. He, M. Kurachi, and M. Tanabashi, Phys. Rev. D **71**, 115001 (2005).
[11] R. Casalbuoni, S. D. Curtis, D. Dolce, and D. Dominici, Phys. Rev. D **71**, 075015 (2005).
[12] A. Belyaev, R. S. Chivukula, N. D. Christensen, H. J. He, M. Kurachi, E. H. Simmons, and M. Tanabashi, Phys. Rev. D **80**, 055022 (2009); arXiv:1003.1786.
[13] H. J. He, Y. P. Kuang, Y. Qi, B. Zhang, A. Belyaev, R. S. Chivukula, N. D. Christensen, A. Pukhov, and E. H. Simmons, Phys. Rev. D **78**, 031701 (2008).
[14] T. Ohl and C. Speckner, Phys. Rev. D **78**, 095008 (2008); T. Abe, T. Masubuchi, S. Asai, and J. Tanaka, Phys. Rev. D **84**, 055005 (2011); F. Bach and T. Ohl, Phys. Rev. D **85**, 015002 (2012).
[15] R. Casalbuoni, S. De Curtis, D. Dominici, and R. Gatto, Phys. Lett. **155B**, 95 (1985).
[16] R. Casalbuoni, D. Dominici, A. Deandrea, R. Gatto, S. De Curtis, and M. Grazzini, Phys. Rev. D **53**, 5201 (1996).
[17] M. Bando, T. Kugo, S. Uehara, K. Yamawaki, and T. Yanagida, Phys. Rev. Lett. **54**, 1215 (1985).
[18] M. Bando, T. Kugo, and K. Yamawaki, Nucl. Phys. **B259**, 493 (1985).
[19] M. Bando, T. Fujiwara, and K. Yamawaki, Prog. Theor. Phys. **79**, 1140 (1988).
[20] M. Bando, T. Kugo, and K. Yamawaki, Phys. Rep. **164**, 217 (1988).
[21] M. Harada and K. Yamawaki, Phys. Rep. **381**, 1 (2003).
[22] J. M. Cornwall, D. N. Levin, and G. Tiktopoulos, Phys. Rev. Lett. **30**, 1268 (1973); Phys. Rev. D **10**, 1145 (1974); C. H. Llewellyn Smith, Phys. Lett. **46B**, 233 (1973); D. A. Dicus and V. S. Mathur, Phys. Rev. D **7**, 3111 (1973); B. W. Lee, C. Quigg, and H. B. Thacker, Phys. Rev. Lett. **38**, 883 (1977); Phys. Rev. D **16**, 1519 (1977); M. S. Chanowitz and M. K. Gaillard, Nucl. Phys. **B261**, 379 (1985).
[23] R. S. Chivukula, H. J. He, M. Kurachi, E. H. Simmons, and M. Tanabashi, Phys. Rev. D **78**, 095003 (2008).
[24] K. Hagiwara and D. Zeppenfeld, Report No. DESY-85-133 (unpublished); K. Hagiwara, R. D. Peccei, D. Zeppenfeld, and K. Hikasa, Report No. DESY-86-058, 1986 (unpublished); K. Hagiwara and D. Zeppenfeld, KEK, Report No. 87-158, 1988.
[25] A. Pukhov, E. Boos, M. Dubinin, V. Edneral, V. Ilyin, D. Kovalenko, A. Kryukov, V. Savrin *et al.*, arXiv:hep-ph/9908288.
[26] A. Pukhov, arXiv:hep-ph/0412191.
[27] N. D. Christensen and C. Duhr, Comput. Phys. Commun. **180**, 1614 (2009).
[28] N. D. Christensen, P. de Aquino, C. Degrande, C. Duhr, B. Fuks, M. Herquet, F. Maltoni, and S. Schumann, Eur. Phys. J. C **71**, 1541 (2011).
[29] J. Pumplin, D. R. Stump, J. Huston, H. L. Lai, P. Nadolsky, and W. K. Tung, J. High Energy Phys. 07 (2002) 012.
[30] This kind of cut should be applied to separated jets. Experimentally, two jets are separable if $\Delta R_{jj} > 0.5$ [see for instance, S. Ask (ATLAS Collaboration), arXiv:1106.2061], and two jet-cones do not overlap at all if $\Delta R_{jj} > 1$. So the cut in Eq. (9) can be realized.
[31] K. Nakamura *et al.* (Particle Data Group), J. Phys. G **37**, 075021 (2010).